RSC Advances

PAPER

View Article Online
View Journal | View Issue

Cite this: *RSC Adv.*, 2025, **15**, 41537

Green synthesis of coconut coir-based carbon dots for efficient detection of ferric ions

Shalni Srivastava,[a] Aneesh Ali,[a] Kanika,[a] Prodipta Samadder,[b] Bhuvnesh Kumar,[a] Awdhesh Kumar Mishra,*[c] Mohammad Rashid Khan,[d] Nemat Ali,[d] Young-Ok Son*[e] and Rehan Khan*[a]

Received 18th May 2025
Accepted 21st October 2025

DOI: 10.1039/d5ra03499j

rsc.li/rsc-advances

Iron (Fe) is an essential micronutrient for metabolic and physiological processes. Its dysregulation is associated with disorders such as Alzheimer's and hemochromatosis. Therefore, the development of cost-effective and selective probes for Fe(III) detection is of significant clinical importance. In this study, fluorescent carbon dots derived from coconut coir (CCDs) were synthesized *via* a single-step hydrothermal method. The CCDs exhibited strong blue emission at 450 nm under 350 nm excitation and demonstrated selective fluorescence quenching in the presence of Fe(III) ions, with a detection limit of 223.2 μM. HR-TEM revealed the particle size of CCDs ranged between 5.64 to 10 nm. XRD confirmed the crystalline nature. FTIR spectra indicated presence of hydroxyl and carboxyl groups contributing to dispersibility and surface passivation. Raman spectroscopy showed distinct D (1354 cm^{-1}) and G (1582.61 cm^{-1}) bands, characteristic of low-dimensional carbon nanostructures. Bioimaging and cytocompatibility studies in L929 fibroblast cells confirmed biocompatibility up to 500 μg mL^{-1}. Collectively, these findings highlight the potential of CCDs as an effective fluorescent probe for Fe(III) sensing and bioimaging applications in medical diagnostics. The CCDs were cytocompatible at concentrations up to 500 μg mL^{-1}

1. Introduction

Iron is an essential micronutrient involved in critical cellular functions such as the electron transport chain, transcriptional regulation of genes, enzymatic catalysis, and oxygen transport.[1] It is also a key component of biologically significant proteins such as hemoglobin and myoglobin, additionally, iron relates to neurobiological functions such as synaptogenesis and myelination. Dysregulation of iron homeostasis can result in severe health disorders, including hemochromatosis,[2] hemosiderosis,[3] Alzheimer's disease,[4] ferroptosis,[5] anemia,[6] and liver damage.[7,8]

Thus, it is essential to detect Fe(III) levels in biological systems with a high degree of selectivity and sensitivity. Various analytical techniques are commonly used for iron detection, such as atomic absorption spectroscopy, voltammetry analysis, inductively coupled plasma mass spectrometry, ion pair chromatography *etc.* These techniques are widely recognized for their high sensitivity, reproducibility and precise diction. However, these methods are often constrained by limitations, including costly instrumentation, requirement of skilled operator, and intricate, time-intensive protocols. Consequently, there is an increasing demand for alternative methods that can overcome these challenges.[9,10] Therefore, optical spectroscopy techniques have emerged as a promising alternative with advantages such as being cost-effective, providing operational simplicity and improved selectivity.[11] Fluorescent sensors provide rapid on-site detection and portability.[12] They are extensively utilized for environmental monitoring, food safety assessment, detection of metal ions, biomolecules, cancer cells, pesticides and explosive materials.[2]

Carbon dots have gained significant interest as new-generation fluorescent sensing probes owing to their distinctive photoluminescent properties. They also exhibit low toxicity, high chemical stability, minimal photobleaching and excellent biocompatibility, these properties support their use in clinical diagnostic applications. Li *et al.* for the first time prepared carbon dots (CDs) from *Bacillus cereus* using simple single-step hydrothermal process for the selective detection of *p*-nitrophenol. They also injected the synthesized CDs into male BALB/c mice and reported their excellent biocompatibility.[13] Karak

[a]*Chemical Biology Unit, Institute of Nano Science and Technology, Knowledge City, Sector-81, Mohali-140306, Punjab, India. E-mail: rehankhan@inst.ac.in*

[b]*Energy and Environment Unit, Institute of Nano Science and Technology, Knowledge City, Sector-81, Mohali-140306, Punjab, India*

[c]*Department of Biotechnology, Yeungnam University, Gyeongsan 38541, South Korea*

[d]*Department of Pharmacology & Toxicology, College of Pharmacy, King Saud, University, P.O. Box 2457, Riyadh 11451, Saudi Arabia*

[e]*Department of Animal Biotechnology, Faculty of Biotechnology, College of Applied Life Sciences and Interdisciplinary Graduate Program in Advanced Convergence Technology and Science, Jeju National University, Jeju 63243, Republic of Korea. E-mail: sounagi@jejunu.ac.kr; Tel: +82-64-754-3331*

et al. reported procedure to synthesis CDs with high yield from natural source. Heating banana juice at 150 °C without any surface passivating or oxidizing agents for four hours produced water-soluble, green luminescent, carbon dots with an average particle size of 3 nm.[14] Chanthai *et al.* proposed green synthesis of Self-functional CDs from shallot; heated four hours at 180 C in a Tefon-lined autoclave for detection of Cr(III) and Cr(VI) ions.[15] Huang *et al.* studied the interaction between the synthesized nitrogen doped CDs from various natural precursors and their selectivity towards mercury ions in order to determine the dependency of interactions on the surface states of the CDs.[16] Zhao *et al.* reported green synthesis of nitrogen doped carbon quantum dots (CQDs) *via* solvo-thermal treatment from bran and tartaric acid. Green emissive CQDs were utilized for the selective detection of Cu^{2+} ions in water samples.[17] Tong *et al.* synthesized nitrogen and sulfur co-doped carbon quantum dots from citric acid and cysteine as precursors to enhance the electron transfer efficiency and strengthen the coordination interaction between *N*,*S*-CQDs and Fe(III) ions.[18] Emadi *et al.* and Kim *et al.* proposed microwave method for fabricating Fe-doped carbon quantum dots[19] and solvothermal method for the synthesis of green-emissive carbon quantum dots[20] respectively. Both the studies reported a quantum yield of ~18%. Lee *et al.* reported synthesis of graphitic carbon quantum dot utilizing the electrochemical ablation method.[21] Zhu *et al.* prepared carbon quantum dots using tetraacetic acid salts and ferric nitrate with a quantum yield of 16.23%.[22] The proposed work showcases synthesis of carbon dots from waste biomass (coconut coir) therefore proposing upcycling of waste materials with a higher quantum yield without the requirement of doping to promote the coordination interaction and electron transfer among CCDs and metal ions.

In present work coconut coir was utilized as a natural precursor to synthesis carbon dot using a single-step hydrothermal route. The carbon dots exhibited bright blue fluorescence emission at 450 nm under 350 nm excitation. Its structural properties were investigated by HR-TEM, XPS, XRD, Raman and FT-IR. While the optical properties were determined *via* UV-Vis and PL spectroscopy. The CCDs were directly utilized as rapid and highly selective fluorescent probes to detect Fe(III) ions without any functional modification. Their bioimaging and cytocompatibility were investigated in the L929 cells.

2. Experimental details

2.1. Materials

Coconut coir (*Cocos nucifera* L.) was purchased from a local market (Mohali, India). Zinc(II) sulfate heptahydrate, ferrous(III) chloride tetrahydrate, ferric(II) chloride, arsenic(III) trichloride, manganese(II) chloride, mercury(II) chloride, chromium(III) nitrate, vanadium(III) chloride, quinine sulfate salt, MTT were purchased from Sigma-Aldrich. L929 mouse fibroblast cell line was purchased from the NCCS Pune, India. Ammonium(I) chloride, copper(II) nitrate, were obtained from TCI. Nickel(II) chloride, palladium(II) chloride, lead(II) chloride, potassium(I) chloride from SRL. Silver(I) nitrate, aluminium(III) chloride, barium(II) chloride, cadmium(II) chloride, cobalt(II) chloride were procured from Loba Chemie Pvt. Ltd. Calcium(II) chloride from Himedia, and magnesium(II) sulfate heptahydrate, sodium(I) nitrite from Emparta. All chemical utilized were analytical reagent grade with 99% purity and the glassware used in the experiments was obtained from Harco.

2.2. Methods

2.2.1. Synthesis of photoluminescent CCDs. A single-step hydrothermal procedure was used to synthesize the CCDs. In brief the process involved numerous steps, including decarboxylation, hydrolysis, polymerization, and dehydration. The coconut coir was cut into small pieces with a sterile knife and ground to a fine powder for use in CCD synthesis. 20 g coir powder was put in a silica crucible and heated to 600 °C in a nitrogen environment for 3 h using a muffle furnace (Metrex). After cooling, the silica crucible containing a black powder was removed from the furnace. The resulting powder was thoroughly crushed to tiny carbon particles using mortar and pestle. Finely crushed particles (0.5 g) were added to 100 mL of deionized water and stirred continuously for 18 h. The aggregated particles were removed by centrifuging (Eppendorf centrifuge 5804) at 5000 rpm, temperature 25 °C for 8 min. The supernatant was filtered by using 0.2 μm filter and stored at 25 °C temperature for further analyses.

2.2.2. Structural, optical characterization and sensing measurements. This study employed a range of analytical techniques to investigate the structural and optical properties of CCDs. High-resolution transmission electron microscopic (HR-TEM) images were obtained using a JEOL JEM-2100 HR-TEM instrument operating at 200 kV to describe the particle size and morphology of the synthesized CCDs. Diluted samples were sonicated and drop-casted on Cu-coated carbon grids for the analysis. X-ray photoelectron (XPS) spectra using an ESCALAB 250Xi spectrometer (Thermo Fisher Scientific) was recorded to analyze the surface sensitive chemical and elemental composition of CCDs. X-ray diffractometer (XRD, Bruker Eco D8) with Cu Kα radiation ($\lambda = 0.154056$ nm) and fine-focus filament was used as a cathode and a Cu anode was used as the target material to determine the crystallinity of CCDs. A Bruker spectrophotometer with ZnSe crystal was employed to determine the Fourier transform infrared (FT-IR) spectrum with air scan as background. The Raman spectra were recorded using a confocal Raman system (WITec) coupled with a 532 nm laser source and the optical properties of CCDs were determined by a UV-Vis absorption spectra (200–800 nm) obtained using a Shimadzu UV-Vis 2600, whereas the emission spectra were recorded with an Edinburgh FS 5 spectrophotometer at room temperature. All measurements were repeated three times. The standard approach was used to estimate the quantum yield (Q) using quinine sulfate in 0.1 M H_2SO_4 ($Q = 55\%$, excited at 350 nm, $\eta = 1.33$) as ref. 23. The following equation was used to calculate the quantum yield of CCDs:

$$Q(\mathrm{CCD}) = Q(\mathrm{Ref}) \times \frac{I(\mathrm{CCD}) \times A(\mathrm{Ref}) \times \eta^2(\mathrm{CCD})}{I(\mathrm{Ref}) \times A(\mathrm{CCD}) \times \eta^2(\mathrm{Ref})}$$

where; Q stands for the quantum yield, I for the emission intensity, A for the absorbance, and η for the refractive index of the solvent, Ref stands for reference standard, that is, quinine sulfate in 0.1 M H_2SO_4 (Q = 0.55) and CCD stands for the synthesized carbon dots. To evaluate the selectivity of synthesized CCDs, various metal ions, such as Ag(I), Al(III), Ba(II), Cd(II), Co(II), Cu(II), Ca(II), Fe(III), Hg(II), K(I), Mg(II), Na(I), NH_4(I), Ni(II), Pd(II), Zn(II), Pb(II), Fe(II), As(III), Mn(II), Cr(III) and V(III) were individually dissolved in deionized water to prepare 1 mM metal ion solutions. For each test, at room temperature all the metal ions were separately added to the solution of CCDs and the fluorescence spectra were then recorded using a fluorescence spectrophotometer. Furthermore; to assess the sensitivity of CCDs, Fe(III) ion solution of varying concentrations (pH 7) were added to the CCDs solution at room temperature. The fluorescence intensity was then measured at an excitation wavelength of 350 nm. The cytocompatibility of CCDs was measured using L929 cells *via* the 3-(4,5-dimethylthiazol-2-yl)-2,5-diphenyltetrazolium bromide (MTT) assay. The cells were seeded at a density of 1×10^4 in a 96-well plate. The cells were treated with various concentrations of CCDs for 24 and 48 h. The cytocompatibility of CCDs was determined using a slight modification in the protocol provided with the assay kit (Invitrogen). The cells were incubated with MTT for 4 h, and the percentage cell viability was calculated by measuring the absorbance at 570–595 nm. Stock solution of CCDs containing Fe(III) was prepared. This solution was serially diluted with deionized water to a final concentration of 920 μM. One millilitre of CCDs was added to 2 mL of the ion solution, and the fluorescence intensity was measured immediately. The photoluminescence (PL) spectra of CCDs were acquired at an excitation wavelength of 350 nm in the presence and absence of Fe(III).

3. Results and discussion

3.1. Synthesis and structural characterization of CCDs

The CCDs was prepared by simple hydrothermal synthesis using coconut coir as precursor (Scheme 1), avoiding the use of strong acids or organic reagents. The synthesized CCDs exhibited excellent water solubility, producing a golden-brown transparent solution without any agglomeration. We used different biophysical techniques to characterize the CCDs such as HR-TEM which revealed the morphology and size distribution of the synthesized CCDs (Fig. 1a) consisting the average particle diameter to be in the range of 5.64–10 nm. This indicated that the synthesized CCDs were highly pure carbon dots. To confirm the crystalline characteristics of synthesized CCDs XRD analysis was performed which depicted the peaks at (003), (200), (100), and (010) diffraction planes in CCDs which are present at 2θ of 28.37, 40.54, 50.20, and 58.65, respectively (Fig. 1c). Furthermore, the presence of first three peaks represents the presence of sp^2 carbon and the last one corresponds to the sp^3 carbon.[24] Further, to determine the bonding in CCDs Raman spectra was determined, which displayed peak at 1354 cm^{-1} related to the D-band and 1582.61 cm^{-1} corresponding to the G-band (Fig. 1d) confirming the presence of C–C bonds. The G-band represents the in-plane vibrations of sp^2-bonded carbon atoms, whereas the D-band represents the out-of-plane vibrations attributed to the presence of structural defects which is in close agreement with the studies reported.[24] The I_D/I_G ratio (0.982) of the CCDs is less than 2 which indicates the nanocrystalline nature of the carbon dots. XPS analysis of the prepared CCDs revealed the presence of O, N, and C. The wide-range spectrum (Fig. 1b) showed the presence of oxygen (O_{1s}, 533.08 eV), nitrogen (N_{1s}, 400.08 eV), and (C_{1s}, 286.08 eV), which is consistent with the characteristic peaks observed in carbon dots synthesized from biomass.[25] FTIR spectroscopy was used to detect the functional groups in CCDs. The analysis revealed presence of several carboxylic groups (COO^-) with peaks at 1608 and 1353 cm^{-1}. The O–H stretching vibration peak was around 3301.53 cm^{-1} and the –CH stretching mode peak was at 2927 cm^{-1} (Fig. 1e). The poly hydroxyl groups in the coconut coir (lignocellulose) could have contributed to the hydroxyl and carboxyl peaks which provides excellent water solubility of CCDs and a good stability for various biomedical applications.[24,26]

3.2. Optical properties of CCDs

The CCD solution exhibited golden-brown color when placed under white light and when placed under 365 nm UV light, it exhibited bright blue emission, indicative of the fluorescent properties of the synthesized CCDs. The UV-Vis spectrum revealed a strong, broad absorbance band ranging from 236 to 400 nm, with a very slight hump at 248 nm (Fig. 2a) which could be attributed to the π–π* molecular orbital transition of the C=C (alkene) bonds. Additionally, the absorbance in the range of 277–280 nm were due to the n–π* molecular orbital transition of the C=O (carboxyl) functional group, although these

Scheme 1 Schematic of synthesis route for the fluorescent CCDs.

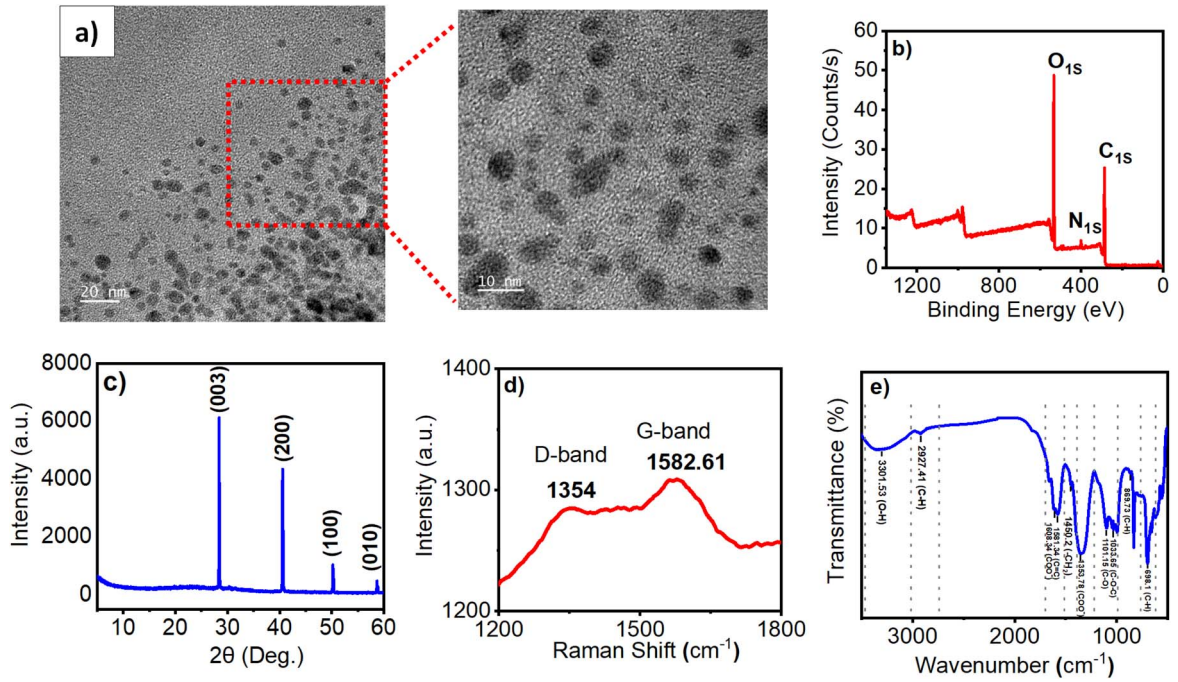

Fig. 1 Morphological and structural characterization of the CCDs. (a) HR-TEM images of CCDs. Enlarge view of HR-TEM images at scale bar 10 nm. (b) Full-survey XPS spectrum, (c) XRD pattern, (d) Raman spectrum and (e) FT-IR spectra of CCDs.

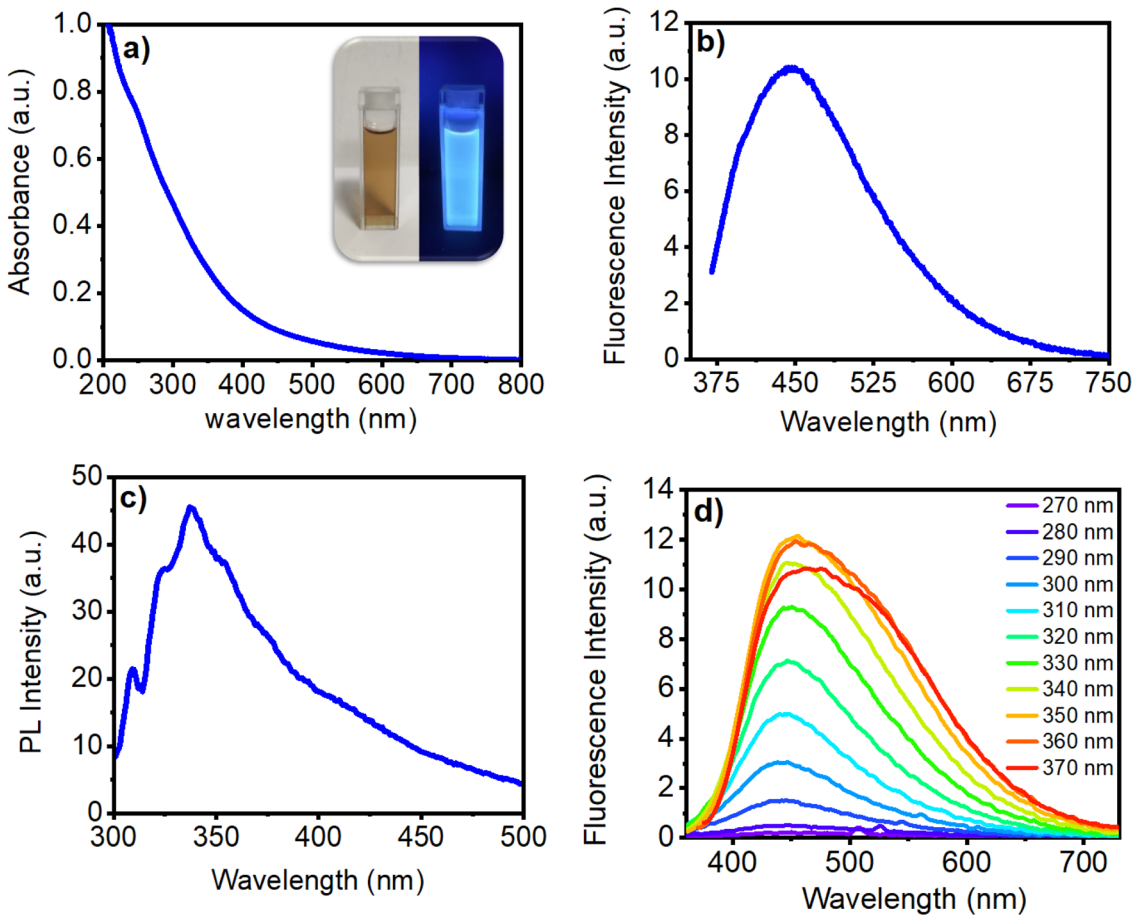

Fig. 2 Photophysical properties of CCDs. (a) UV-Vis absorption, (b) fluorescence spectra, (c) excitation spectra and (d) excitation dependent emission spectra of CCDs. (inset) Under white light and UV light images of CCDs.

peaks are merged within the broad absorption range.[27,28] The fluorescence emission spectra were recorded at an excitation wavelength of 350 nm, revealing an emission maximum at 450 nm (Fig. 2b). The excitation spectrum of the CCDs showed an excitation maximum at 337 nm (Fig. 2c), which was considered optimal for probing the absorbance characteristics of the CCDs. This comprehensive optical analysis confirmed that the synthesized CCDs possessed desirable optical and fluorescence properties. The excitation dependent photoluminescence behavior of CCDs was investigated using fluorescence spectroscopy across excitation wavelengths ranging from 270 to 370 nm (Fig. 2d). The highest emission intensity was recorded at an excitation wavelength of 350 nm, corresponding to an emission peak at 450 nm. Consequently, subsequent fluorescence emission analyses were conducted using 350 nm as the excitation source. The observed variation in emission intensity is attributed to the increased population of CCDs being excited at specific wavelengths. This wavelength dependent emission behavior is ascribed to the effective surface passivation in the synthesized CCDs and to the effect of quantum confinement.[29]

3.3. Quantum yield and lifetime measurement

The fluorescence quantum yield of the synthesized CCDs was determined at an excitation wavelength of 350 nm; quinine sulfate was used as a reference. The CCDs exhibited a quantum yield of 45% which is in close agreement with that reported previously,[27] indicating significantly high emission at 450. The color of the emission of CCDs was found to be bright blue with Commission Internationale de l'Elcairage (CIE) color coordinates of $(x = 0.21, y = 0.23)$ as demonstrated by the chromaticity diagram (Fig. 3a). In addition, the fluorescence decay time of the synthesized CCDs was measured (Fig. 3b). The decay curve of the blue-emitting CCDs was fitted using a biexponential function. The fluorescence decay lifetimes were 1.53 ns (55%) and 5.35 ns (44%), resulting in an average decay lifetime of 4.33 ns. This relatively short lifetime suggests efficient radiative recombination processes, which are indicative of the excellent photophysical properties of the carbon dots.

3.4. Detection of Fe(III) ions with CCDs

To determine the capability of synthesized CCDs to be used as a fluorescent probe for Fe(III) detection we investigated its absorption and emission behavior in the presence of various metal ions. 1 mM concentration of solutions of Ag(I), Al(III), Ba(II), Cd(II), Co(II), Cu(II), Ca(II), Fe(III), Hg(II), K(I), Mg(II), Na(I), NH_4(I), Ni(II), Pd(II), Zn(II), Pb(II), Fe(II), As(III), Mn(II), Cr(III) and V(III) ions were separately added to the CCD solution and the resulting changes in fluorescence spectra were recorded at 450 nm with excitation wavelength of 350 nm. The addition of Fe(III) ions resulted in complete quenching approximately 99% of fluorescence emission. This could be attributed to the surface functional groups on the CCDs such as –OH, –COOH, which can form strong coordination complexes with Fe(III), enabling selective detection.[30] A progressive decrease in fluorescence emission intensity was seen with increase in the concentration from 50 μM to 1 mM of Fe(III) ions. In contrast, the introduction of other trivalent ions such as Cr(III) and V(III) led to partial fluorescence quenching, with reduction of approximately 51.18% and 42.59% respectively (Fig. 4a–c). All the other ions exhibited minimal effect on the fluorescence quenching of CCDs and the absence of significant spectral changes upon exposure to most of the ions suggests that the CCDs exhibit high selectivity toward Fe(III).

Further to evaluate the limit of detection (LoD) fluorescence titration of the CCDs was conducted by incubating them with varying concentrations of Fe(III) solution, ranging from 50 μM to 1 mM (Fig. 4d). The LoD was calculated to be 223.2 μM. The CCDs were synthesized from coconut coir, a natural, economical, biodegradable, renewable and sustainable precursor without any additional surface passivation or utilization of oxidizing agents to enhance the coordination interaction and

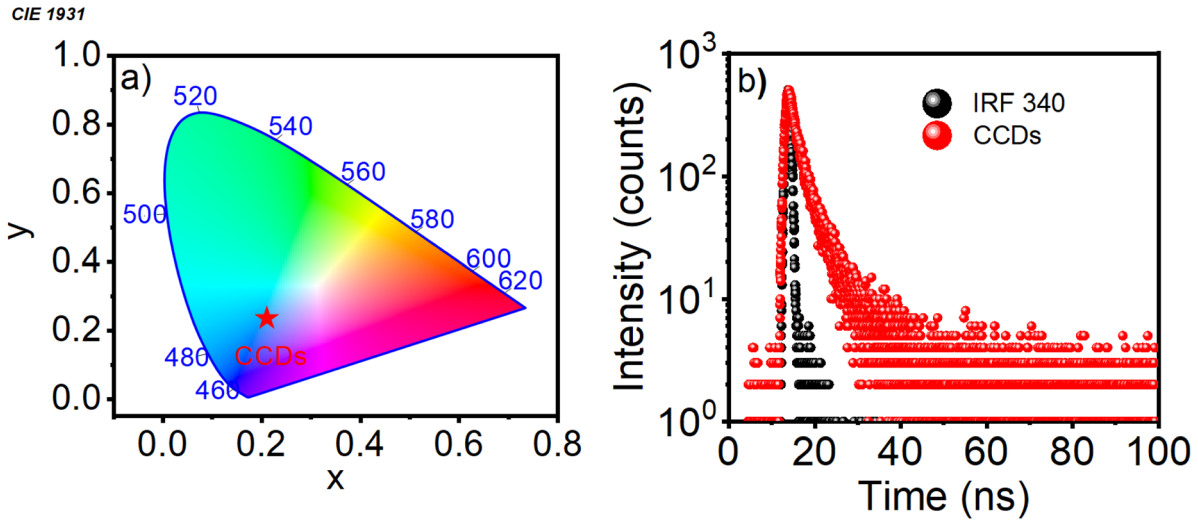

Fig. 3 (a) CIE plot and (b) fluorescence lifetime of CCDs.

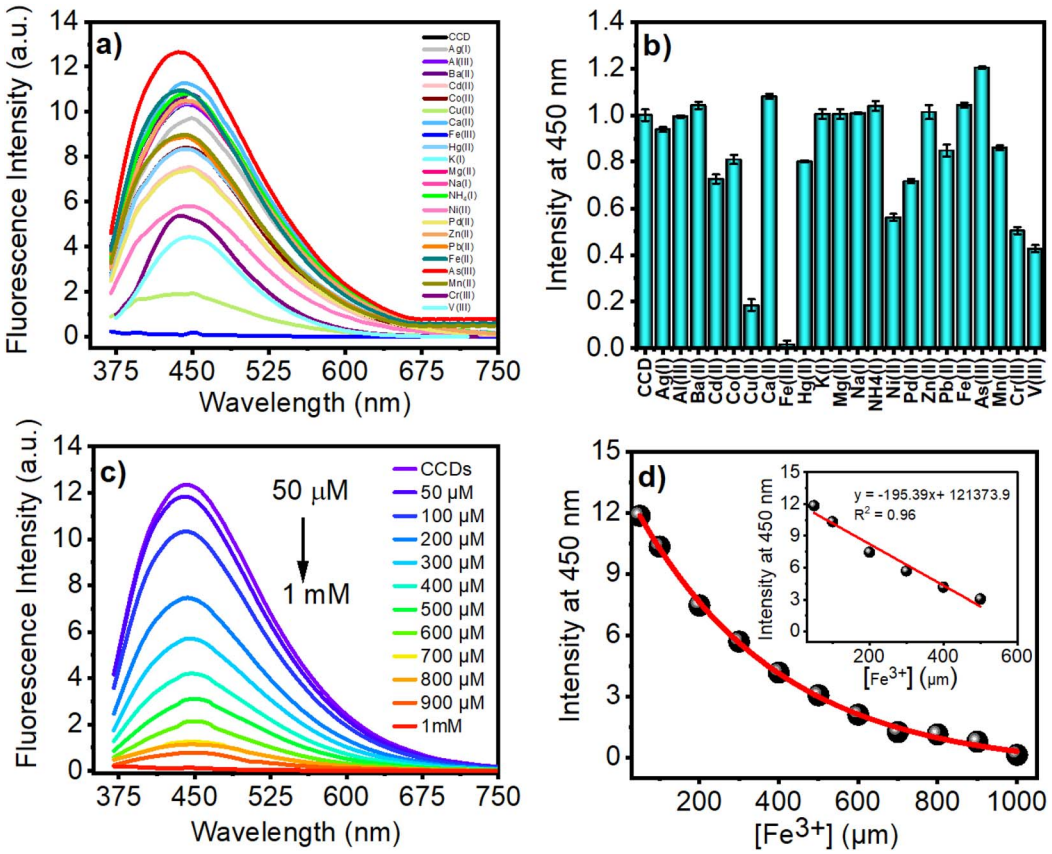

Fig. 4 Selectivity plot of different metal ions on CCDs: (a) fluorescence intensity, (b) fluorescence quenching rate at 450 nm. (c) Fluorescence emission plot of CCDs at different concentration of Fe(III) ions. (d) Limit of detection (LOD) plot of CCDs.

electron transfer among CCDs and Fe(III) ions. It may have resulted in heterogeneous surface states and a relatively low density of surface functional groups compared to surface passivated carbon dot-based probes[16–19] and other synthetically developed probes (Table 1). Simple single-step hydrothermal route was adopted for the synthesis, compared chromenylium–cyanine NIR fluorescent probe[31] involving expensive synthetic dye as precursor, complex synthesis steps and can undergo photobleaching under prolonged exposure like Coumarin Derivatives.[32] While the *Pterocarpus* wood-based fluo-hydrogels[33] can be unstable and the fluorescent properties may fade in light or oxidative environments. 2-Phthalimidobenzoic acid fluorescent probes[34] contain aromatic structures hence interference with other metal ions may lower the selective detection capabilities of the probe. Bromine containing calorimetric Fe(III) detectors such as 6-(6-bromopyridin-2-yl)benzo[4,5]imidazo[1,2-*c*]quinazoline[35] involve multi step synthesis and are not biocompatible. Whereas the synthesized CCDs provides significant advantage of biocompatibility, selectivity and cost-effectiveness towards Fe(III) detection for practical applications in clinical diagnostics.

3.5. Method validation

The plot of fluorescence intensity *versus* different Fe(III) concentration (Fig. 4d) revealed a linear relationship with a high correlation coefficient ($R^2 = 0.968$) and the Stern–Volmer

Table 1 Summary of recent reported methods in literature for the detection of Fe(III) ions

Detection method	Sensing material	Detection mechanism	LoD	Reference
Ultraviolet-visible detection, fluorescence detection	Chromenylium–cyanine near-infrared fluorescent probe	Pale-yellow to green, turn-on fluorescence emission	79.7 nM 24.0 nM	14
Colorimetric, fluorescence probe	Coumarin derivatives	Yellow to shallow orange, turn-on fluorescence emission	4.88×10^{-7} M	15
Fluorescence	*Pterocarpus* wood-based fluo-hydrogels	Quenching	1.17 μM	16
Fluorescence	2-Phthalimidobenzoic acid	Quenching	3.73 μM	17
Calorimetric	6-(6-Bromopyridin-2-yl)benzo[4,5] imidazo[1,2-*c*]quinazoline	Colorless to yellow	53.39 nM	18
Fluorescence	Coconut coir-based carbon dots	Quenching	223.2 μM	This work

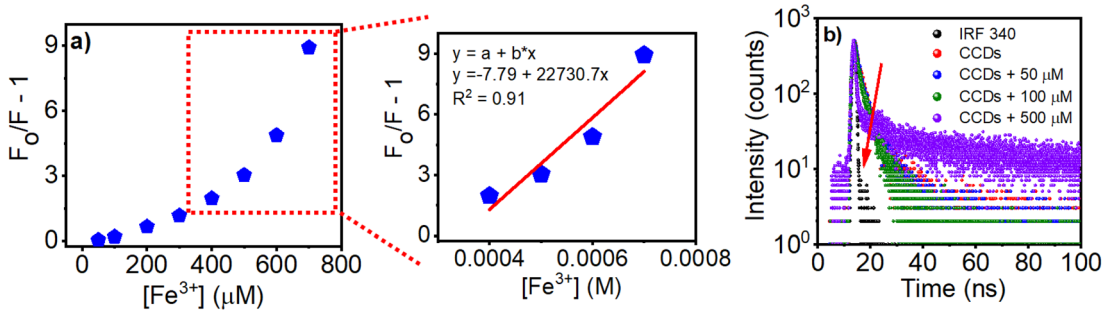

Fig. 5 (a) Stern–Volmer plot of CCDS titrated by different concentration of Fe(III) ions and enlarge view of Stern–Volmer plot at higher concentration of Fe(III) ions. (b) The effect of different concentrations of Fe(III) ions on the fluorescence decay curves of CCDs.

quenching constant (K_{sv}) of the synthesized CCDs by Fe(III), was determined using the following Stern–Volmer (SV) equation:[36]

$$\frac{F_0}{F} = 1 + K_{SV}[Q]$$

where the $\frac{F_0}{F}$ ratio showed fluorescence intensities of before and after the addition of Fe(III) ions, [Q] is the quencher concentration; 50 μM–1 mM of Fe(III) ions in this study.

As observed the fluorescence is quenched with increase in the concentration (50 μM to 1 mM) of Fe(III) ions. The Stern–Volmer plots depicted two distinct regions: at lower concentration of Fe(III) ions linear variation is observed because of static quenching whereas deviation from linearity with increasing concentrations of Fe(III) ions (Fig. 5a) was observed, which could be attributed to dynamic quenching *via* electron transfer or energy transfer between CCDs and Fe(III) ions.[37] The K_{sv} value was calculated to be 2.23×10^4 M^{-1}, indicating a strong quenching efficiency of CCDs toward Fe(III) ions compared with those of most efficient fluorescent molecules.

Further the effect of varying Fe(III) ion concentrations on fluorescence lifetime of CCDs were investigate. The average fluorescence lifetime of CCDs was 4.33 ns and a gradual decrease in the fluorescence lifetime of CCDs occurred with increase in the concentration of Fe(III) ions (Fig. 5b). The fluorescence life of 4.17 ns, 3.655 ns and 1.51 ns was observed for 50, 100 and 500 μM concentration of Fe(III) ions respectively. At low concentrations of Fe(III) ions, the fluorescence lifetime at 450 nm decreases gradually however as the concentration increases rapid decrease is observed; which directly aligns with Fe(III) concentration dependent fluorescence studies (Fig. 4c). This signifies the combined effect of both static and dynamic quenching of fluorescence intensity at varying concentrations of Fe(III) ions; which could be attributed to the formation of stable CCDs/Fe(III) complexes and electron transfer from the excited state of the CCDs to Fe(III) ions respectively.[37] These results validate the interaction between CCDs and Fe(III) ions, enabling high selective detection and their utilization as a fluorescent probe for clinical diagnostic applications.

3.6. *In vitro* stability assay of CCDs

It is essential to assess the *in vitro* cytocompatibility of CCDs to ensure their safety in viable cells. Therefore, we evaluated whether the synthesized CCDs were compatible with L929 cells after 24, 48 and 72 h (Fig. S4) of treatment. An MTT assay was performed to determine cell viability. The CCDs were cytocompatible at concentrations up to 500 μg mL^{-1} and had no significant toxicity in these cells (Fig. 6).[38]

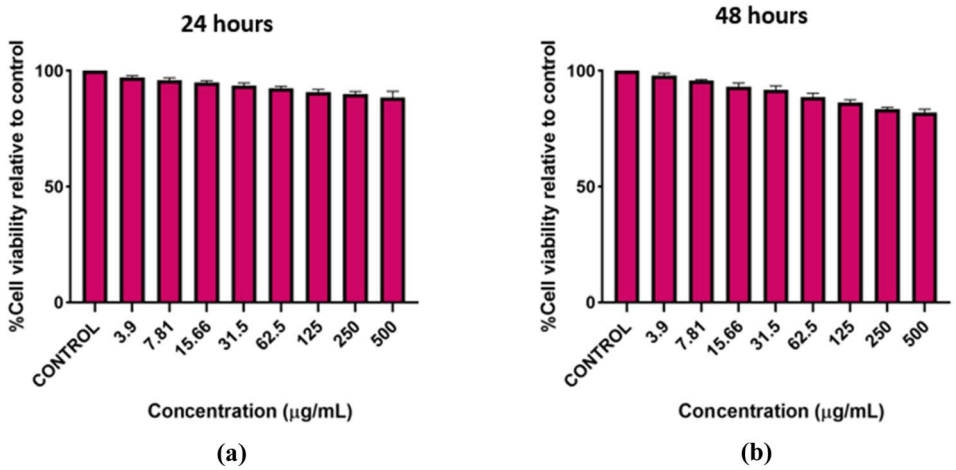

Fig. 6 *In vitro* cytocompatibility of CCDs after (a) 24 and (b) 48 h.

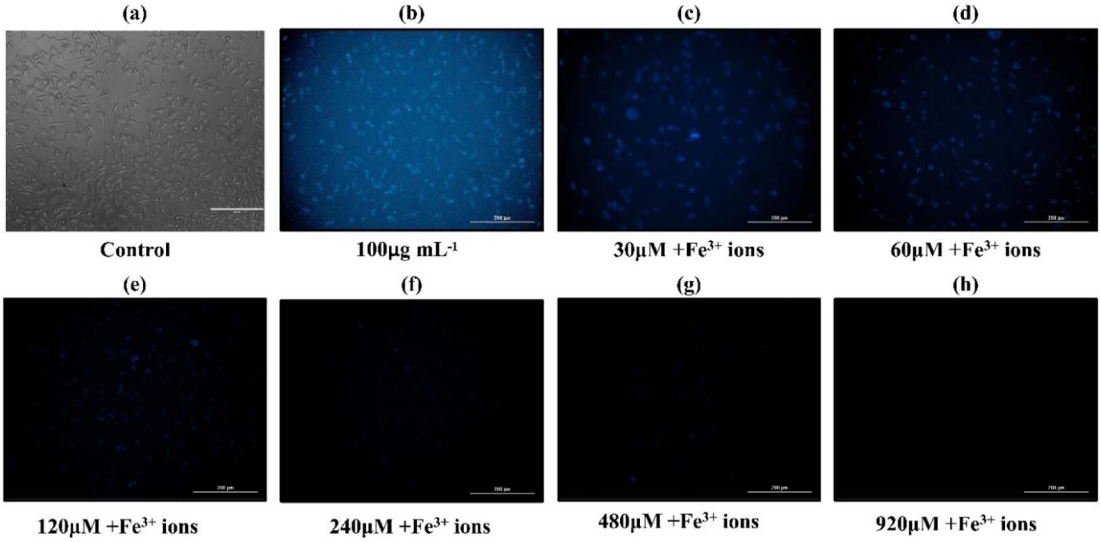

Fig. 7 Fluorescence imaging of L929 cells incubated with CCDs (100 μg mL^{-1}) for 7 h at 37 °C. (a) Control (b) L929 cells were incubated with CCDs and various concentrations of Fe(III) (c) 30 μM, (d) 60 μM, (e) 120 μM, (f) 240 μM, (g) 480 μM, and (h) 920 μM.

3.7. Fe(III) sensing in L929 cells

We checked the practicability of sensing Fe(III) in live cells using the CCDs. L929 cells were co-incubated with CCDs (100 μg mL^{-1}) for 24 h. Thereafter, the cells were examined under a confocal microscope to determine the fluorescence intensity of CCDs. The morphology of L929 cells remained intact and the blue fluorescence was retained, reaching the cell nucleus *via* endocytosis of CCDs. Furthermore, semi-quantitative analysis of the sensing of Fe(III) at various concentrations (30–920 μM) by CCDs was performed by treating the cells with Fe(III).[39] By introducing increasing quantities of Fe(III) ions, the fluorescent signal in the living cells was gradually quenched (Fig. 7). Fluorescence intensity (%) has been quantified *vs.* Fe(III) increasing concentration (μM) in L929 cells with respect to control included in (Fig. S5). These results demonstrate that in living cells Fe(III) can be detected using this fluorescent CCD probe, highlighting its practical application.

4. Conclusion

In this study, waste biomass (coconut coir) was converted into carbon dots (CCDs) *via* single-step hydrothermal process. The CCDs were less than 10 nm in size, exhibited bright blue emission at 450 nm under 350 nm excitation, with a quantum yield of 45%. They were highly water soluble and depicted a broad UV-Vis absorption band, attributed to π–π* and n–π* transitions. The selective and sensitive detection of Fe(III) ions with the synthesized CCDs demonstrated a detection limit of 223.2 μM with a linearity (R^2) = 0.968. The quenching studies revealed synergistic effect of static and dynamic fluorescence quenching. Cytocompatibility assays in L929 cells confirmed stability and low toxicity up to 500 μg mL^{-1}. These results highlight the potential of synthesized CCDs as promising probes for Fe(III) detection, with strong potential for applications in bioimaging, image-guided photodynamic therapy, targeted drug delivery, and optoelectronic biosensing.

Conflicts of interest

There is no conflict of interest to declare among the authors.

Abbreviations

CCDs	Coconut carbon dots
FTIR	Fourier transform infrared spectroscopy
XRD	X-ray diffraction studies
UV-Vis	UV absorption
HR-TEM	High resolution transmission electron microscopy
XPS	X-ray photoelectron spectroscopy

Data availability

The data supporting this article have been included as part of the supplementary information (SI). Supplementary Information: SEAD pattern of synthesized CCDs, photostability studies of CCDs, method validation for fluorescence lifetime plot of CCDs incubated with varying Fe(III) concentrations and *in vitro* cytocompatibility studies. See DOI: **https://doi.org/10.1039/d5ra03499j**.

Acknowledgements

This work was supported by the Anusandhan National Research Foundation (ANRF) (Grant No. CRG/2022/009388). Department of Health Research, Grant in Aid (Grant No. R.11017/23/2023-GIA/HR). This research was supported by the Basic Science Research Program to Research Institute for Basic Sciences (RIBS) of Jeju National University through the National Reseach

Foundation of Korea (NRF), funded by the Ministry of Education (Grant No. RS-2019-NR040080). The authors acknowledge and appreciate the Ongoing Research funding program (ORF-2025-940) King Saud University, Riyadh, Saudi Arabia.

References

1 X. Liu, N. Li, M.-M. Xu, J. Wang, C. Jiang, G. Song and Y. Wang, *RSC Adv.*, 2018, **8**, 34860–34866.
2 R. Khalid, T. Javid, A. Pervaiz, M. A. Assiri, Z. A. Khan, Sania and S. A. Shahzad, *RSC Adv.*, 2025, **15**, 8456–8463.
3 W. Bekhechi, H. Chiali, L. Khelil, R. Sari-Hamidou and M. Benmansour, *Hemodial. Int.*, 2023, **27**, 270–277.
4 D. Tran, P. DiGiacomo, D. E. Born, M. Georgiadis and M. Zeineh, *Front. Hum. Neurosci.*, 2022, **16**, 838692.
5 L. Yao, J. Hou, X. Wu, Y. Lu, Z. Jin, Z. Yu, B. Yu, J. Li, Z. Yang, C. Li, M. Yan, Z. Zhu, B. Liu, C. Yan and L. Su, *Redox Biol.*, 2023, **67**, 102923.
6 O. Dalkilic, E. Bozkurt, F. Lafzi and H. Kilic, *Org. Biomol. Chem.*, 2023, **21**, 5406–5412.
7 S. A. Rupa, M. A. M. Patwary, W. E. Ghann, A. Abdullahi, A. K. M. R. Uddin, Md. M. Mahmud, Md. A. Haque, J. Uddin and M. Kazi, *RSC Adv.*, 2023, **13**, 23819–23828.
8 H. Seung No, M. Sim, I. Shin, J. Kim and J. Hong, *Chem. Asian J.*, 2025, **20**, e202400805.
9 E. Bulska and A. Ruszczyńska, *Phys. Sci. Rev.*, 2017, **2**(5), 20178002.
10 D. Elango, A. Kanatti, W. Wang, A. R. Devi, M. Ramachandran and A. Jabeen, *Commun. Soil Sci. Plant Anal.*, 2021, **52**, 1069–1075.
11 U. M. Pal, M. Saxena, G. K. Anil Vishnu, D. Parsana, B. S. R. Sarvani, M. Varma, M. Jayachandra, V. Kurpad, D. Baruah, G. Gogoi, J. S. Vaidya and H. J. Pandya, *Appl. Spectrosc. Rev.*, 2020, **55**, 778–804.
12 M. Li, Q. Shi, N. Song, Y. Xiao, L. Wang, Z. Chen and T. D. James, *Chem. Soc. Rev.*, 2023, **52**, 5827–5860.
13 S. Zhang, D. Zhang, Y. Ding, J. Hua, B. Tang, X. Ji, Q. Zhang, Y. Wei, K. Qin and B. Li, *Analyst*, 2019, **144**, 5497–5503.
14 B. De and N. Karak, *RSC Adv.*, 2013, **3**, 8286.
15 C. Sakaew, P. Sricharoen, N. Limchoowong, P. Nuengmatcha, C. Kukusamude, S. Kongsri and S. Chanthai, *RSC Adv.*, 2020, **10**, 20638–20645.
16 Y. H. Yuan, Z. X. Liu, R. S. Li, H. Y. Zou, M. Lin, H. Liu and C. Z. Huang, *Nanoscale*, 2016, **8**, 6770–6776.
17 J. Xu, C. Wang, H. Li and W. Zhao, *RSC Adv.*, 2020, **10**, 2536–2544.
18 H. Wu, J. Jiang, X. Gu and C. Tong, *Microchim. Acta*, 2017, **184**, 2291–2298.
19 A. Gholipour, M. Jahanshahi and H. Emadi, *J. Cluster Sci.*, 2024, **35**, 237–251.
20 G. S. Das, J. P. Shim, A. Bhatnagar, K. M. Tripathi and T. Kim, *Sci. Rep.*, 2019, **9**, 15084.
21 Y.-L. Zhang, L. Wang, H.-C. Zhang, Y. Liu, H.-Y. Wang, Z.-H. Kang and S.-T. Lee, *RSC Adv.*, 2013, **3**, 3733.
22 S. Zhuo, Y. Guan, H. Li, J. Fang, P. Zhang, J. Du and C. Zhu, *Analyst*, 2019, **144**, 656–662.
23 V. B. Kumar, S. K. Mirsky, N. T. Shaked and E. Gazit, *ACS Nano*, 2024, **18**, 2421–2433.
24 L. A. A. Chunduri, A. Kurdekar, S. Patnaik, B. V. Dev, T. M. Rattan and V. Kamisetti, *Mater. Focus*, 2016, **5**, 55–61.
25 X. Deng, Y. Feng, H. Li, Z. Du, Q. Teng and H. Wang, *Particuology*, 2018, **41**, 94–100.
26 K. Kirubanithy, D. Ponnalagar and A. Santhanam, *Carbon Lett.*, 2024, **34**, 2013–2026.
27 P. Chauhan, S. Dogra, S. Chaudhary and R. Kumar, *Mater. Today Chem.*, 2020, **16**, 100247.
28 S. Edakkaparamban, M. Kitamura, Y. Ide, K. Umemura and A. Ishizawa, *Mater. Lett.*, 2023, **345**, 134508.
29 X. Li, H. Wang, Y. Shimizu, A. Pyatenko, K. Kawaguchi and N. Koshizaki, *Chem. Commun.*, 2011, **47**, 932–934.
30 A. López-Beltrán, C. Iriarte-Mesa, C. Murru, F. J. Chao-Mujica, A. L. Corcho-Valdés, L. Morales-Álvarez, L. F. Desdín-García, J. Deschamps and M. Antuch, *Chem.–Eur. J.*, 2023, **29**, e202300188.
31 P. Luo, H. Chen, X. Cheng, L. Liu, Y. Yang, H. Wen, B. Hu, D. Zhou and H. Jiang, *Spectrochim. Acta, Part A*, 2025, **343**, 126593.
32 Z.-Y. Yin, J.-H. Hu, K. Gui, Q.-Q. Fu, Y. Yao, F.-L. Zhou, L.-L. Ma and Z.-P. Zhang, *J. Photochem. Photobiol., A*, 2020, **396**, 112542.
33 J. Li, R. Li, W. Leng, Z. Liu and J. Shi, *Chem. Eng. J.*, 2025, **515**, 163887.
34 E. Elbayoumy, M. Shaker, M. Gaafar, E. A. Moawed and M. M. Aboelnga, *J. Photochem. Photobiol., A*, 2025, **466**, 116391.
35 M. Shirzadi-Ahodashti, M. A. Ebrahimzadeh and P. Biparva, *J. Fluoresc.*, 2025, **35**, 7319–7326.
36 Y. Lang, L. Geng, L. Lan, X. Sun and X. Zhang, *Spectrosc. Lett.*, 2018, **51**, 123–129.
37 S. Gao, X. Wang, N. Xu, H. Lian, L. Xu, W. Zhang and C. Xu, *Cellulose*, 2021, **28**, 1647–1661.
38 A. Vyawahare, R. Prakash, C. Jori, A. Ali, S. S. Raza and R. Khan, *ACS Nano*, 2022, **16**, 18579–18591.
39 R. Pratap, N. Hassan, M. Yadav, S. K. Srivastava, S. Chaudhary, A. K. Verma, J. Lahiri and A. S. Parmar, *Environ. Sci.: Nano*, 2024, **11**, 1636–1653.